Int. J. Heat Mass Transfer. Vol. 35, No. 11, pp. 3009–3020, 1992
Printed in Great Britain

0017–9310/92 $5.00 + 0.00

Impingement cooling flow structure and heat transfer along rib-roughened walls

C. GAU and C. C. LEE
Institute of Aeronautics and Astronautics, National Cheng Kung University, Taiwan, Republic of China

(*Received* 3 *June* 1991 *and in final form* 24 *October* 1991)

Abstract—Slot-air-jet impingement cooling flow structure and heat transfer along rib-roughened walls is studied experimentally. The flow structure along the ribbed wall is visualized with smoke that is generated by vaporizing the oil coated over a heated resistance wire. The effect of different rib protrusions (heights) on the impinging flow and heat transfer along the wall is studied, which is achieved by using different sizes of nozzles. Two different ribbed walls with different rib pitches are selected which have a rib pitch-to-height ratio of 3 and 4, respectively. During the experiments, the Reynolds number varies from 2500 to 11 000, the slot width-to-rib height ratio from 1.17 to 6.67, and nozzle-to-plate spacing from 2 to 16. Due to the protrusion of the rib, the formation of an air bubble enclosing the cavity occurs which can prevent the jet from impinging on the wall and reduce the heat transfer. However, some portion of the jet flow in the downstream region, especially when it becomes turbulent, can penetrate the air bubble and impinge, and recirculate inside the cavity, which significantly increases the heat transfer. In general, the flow structure and the heat transfer observed are significantly different from the results of a flat plate. A comparison and correlations of the stagnation point Nusselt number under different conditions are presented and discussed.

1. INTRODUCTION

IMPINGEMENT cooling heat transfer has been studied extensively in the past due to its wide application in cooling the walls of a high temperature thermal system. The air-jet impinging normally on the wall can remove a large amount of heat over a relatively small surface area. It has been frequently used in cooling the hottest section of a combustion chamber or a turbine blade. A good review article on the study of impingement cooling flow and heat transfer is available [1, 2]. The impingement cooling jet from a single rectangular or round nozzle or an array of nozzles over a heated surface has been well studied. Correlations of stagnation point and local average Nusselt number in terms of relevant nondimensional parameters have been obtained [1, 2].

However, the studies in the past are mostly on a flat surface [1–11] with relatively few over a curved surface [12–15]. In a practical situation, the surface which needs to be cooled may not be smooth or flat. In some situations, to enhance the heat transfer, the surface may be roughened. In addition, the surface may become roughened due to unavoidable corrosion or contamination. Therefore, it is interesting to understand the effect of surface roughness on the heat transfer along a roughened wall. The current study considers the configuration of the impingement cooling process over a rib-roughened wall. A review of literature indicates that a study of the current subject is still lacking. Therefore, the objective of the present work is to experimentally study and provide impingement cooling flow structure and heat transfer data along the rib-roughened walls. The heating condition considered is a heated flat wall with the placement of small rib elements. Therefore, the rib elements actually serve as small fins. It is noted that the heating condition in the current work is slightly different from an actual practice, such as turbine blade cooling. The flat wall is heated electrically by passing a current through a 0.015 mm thin stainless steel foil so that a constant heat flux boundary condition along the wall can be achieved. The local Nusselt number distributions along the ribbed wall are measured. The flow structure is visualized with smoke that is generated by vaporizing the oil coated over a heated resistance wire. During the experiment, a total of four nondimensional parameters, i.e. the Reynolds number, the slot width-to-rib height ratio, the nozzle-to-plate spacing and the rib pitch-to-height ratio, that affect the local Nusselt number distribution are selected to vary. For convenience, the variation of the slot width-to-rib height ratio is achieved by using different sizes of nozzle. Two different cases of the impingement cooling process are considered. Case A considers the situation when the cooling jet is directed toward the rib, while case B considers when it is directed toward the center line of the cavity. A comparison and correlations of the stagnation point Nusselt number under different conditions of cooling are made and discussed.

2. EXPERIMENTAL APPARATUS AND PROCEDURES

The impinging air jet issued from the nozzle is supplied with a high pressure blower system which can furnish a maximum air flow of 10 $m^3 min^{-1}$. To ensure air quality, a settling chamber with a honeycomb and

NOMENCLATURE

A	area of heater strip
b	slot width
c_p	specific heat
e	rib height
I	current
k	thermal conductivity
Nu	Nusselt number, $h_1 b/k$
p	rib pitch
Pr	Prandtl number, $c_p\mu/k$
q	heat flux
Re	Reynolds number, $U_j b/\nu$
T	temperature
U	streamwise velocity
V	voltage
x	lateral distance from the stagnation point
Z	slot-to-plate spacing.

Greek symbols

α	thermal diffusivity
μ	viscosity
ν	kinematic viscosity.

Subscripts

aw	refer to adiabatic wall
j	refer to jet flow at slot exit
o	refer to stagnation point
w	refer to wall
∞	refer to ambient air.

different sizes of meshes is made and used to reduce the turbulence intensity and maintain a uniform air flow at the exit. The nozzle is made convergent and curved smoothly which allows rapid acceleration of fluid without the occurrence of flow separation and the generation of turbulence. Therefore, uniform velocity profile associated with a relatively low turbulence intensity across the nozzle width at the exit is obtained. The streamwise turbulence intensity at the nozzle exit is measured with a hot wire anemometer and is found to be less than 0.7% for a Reynolds number ranging from 2500 to 11 000. The jet velocity is measured with a Pitot tube. A total of four different sizes of rectangular nozzles are made, which are 0.35, 0.6, 1.2 and 2 cm in width, respectively. To ensure that the second dimension of the nozzle slot does not affect the slot-jet flow, all the nozzles are made to be long in the direction perpendicular to the nozzle axis which is 15 cm in length.

A schematic of the apparatus is shown in Fig. 1. The test section is a rib-roughened wall and has

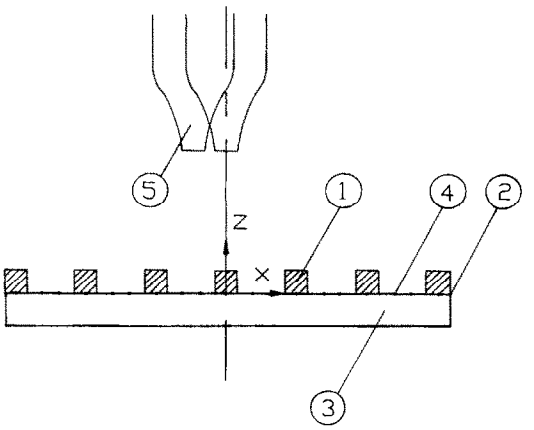

FIG. 1. Schematic of apparatus: (1) square rib, (2) stainless steel foil, (3) Plexiglas plate, (4) thermocouples and (5) rectangular nozzle.

dimensions of 200 mm wide and 400 mm long. It consists of a 5 mm thick Plexiglas, a 0.015 mm thin stainless steel foil which is adhered on the top of the Plexiglas, and a number of 3 mm square rib elements which are mounted and glued in parallel on the foil surface. The ribbed wall can be heated by passing an electric current through the thin stainless steel foil. The layer of glue between the rib and the foil is made thin enough so that the thermal resistance is negligible while the electrical resistance is large enough to prevent the electric current circulating through the ribs. All the ribs are equally spaced. Two different rib-roughened walls having different rib pitches, i.e. 9 and 12 mm, are made, which have a rib pitch-to-height ratio p/e of 3 and 4, respectively. Since the steel foil is so thin and the Plexiglas plate has a very low thermal conductivity, the heat conduction along the plate is negligible. To reduce heat loss to the ambient, the heated roughened wall is well insulated on the back. To account for the additional radiation heat loss directly from both the foil and the ribs, the total heat loss to the ambient is estimated to be less than 3%.

To measure the temperature distribution along the heated wall, a total of 58 thermocouples are inserted individually into a number of equally-spaced small holes drilled in the Plexiglas plate in order to ensure that the thermocouple junction can attach to the heated steel foil. Since all the thermocouples are placed under the ribs (not on top of them), this allows us to study the enhancement of the momentum and heat transfer due to the addition of rib elements on a heated flat plate. The pitch between two adjacent thermocouples is 3 mm. Therefore, there is one thermocouple located at the position where each rib stands. For a ribbed wall having $p/e = 3$, there are two equally spaced thermocouples in each cavity, while for the one having $p/e = 4$, there are three thermocouples in each cavity. One additional thermocouple is used to measure the jet temperature at the slot exit. All the temperature signals are acquired with a data logger

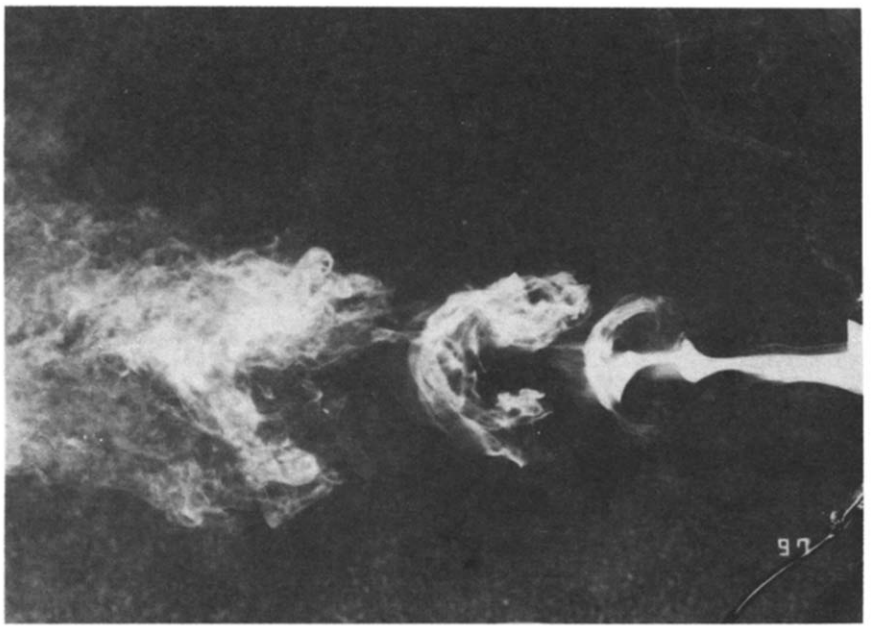

FIG. 2. Typical jet flow structure for $Re = 2500$ and $b = 20$ mm.

and sent into a PC for data processing and plotting. Before the experiments, all the thermocouples are calibrated in a constant temperature bath to ensure a measurement accuracy of $\pm 0.1°C$.

To ensure that the stainless steel foil is heated uniformly, the entire foil is cut into a number of narrow and long strips. Each strip is heated individually with an equal amount of DC power. With the desired voltage V and current I passing through the thin strip, the heat flux along the surface can be calculated and is equal to VI/A, where A is the area of the strip. The local heat transfer coefficient can be determined with the following equation:

$$h_t = q/(T_w - T_\infty). \quad (1)$$

When the air velocity is so high that the wall–air friction can heat up the wall and raise the wall temperature, equation (1) needs to be modified slightly to account for the viscous heating effect. The viscous heating effect becomes noticeable when the impinging jet velocity is greater than 20 m s^{-1}. At this time, T_∞ in equation (1) is replaced with T_{aw}. The adiabatic wall temperature along the surface is measured when the foil heater is turned off.

3. RESULTS AND DISCUSSION

3.1. *Flow visualization*

The jet flow structure and its mixing with ambient air is identical to the one observed in the refs. [9, 15, 16], except in the region close to and along the rib-roughened wall. The jet flow structure can be divided into three different regions, i.e. the potential core, the mixing region and the fully developed turbulence region. A typical jet flow structure is shown in Fig. 2 where vortex formation and pairing due to the mixing of the free jet with the ambient can be observed clearly. Heat transfer process along the wall can be changed significantly when a different region of the jet flow structure impinges on the wall. The maximum in heat transfer occurs when the nozzle-to-plate spacing z/b is close to 8 and the jet flow starts to become fully turbulent. For a higher value of z/b, the jet width becomes so wide before arriving at the wall that the average velocity impinging the wall reduces significantly. This leads to a reduction of heat transfer. For $z/b > 8$, the wall heat transfer decreases monotonically with increasing z/b. In addition, it has been found by Gau and Chung [15] that the increase in the slot width causes an earlier initiation of vortices in the mixing region of the jet which can increase the rate of mixing of the jet flow with the ambient air and result in the enhancement of heat transfer along the wall, especially on the stagnation point.

For impingement cooling over the ribbed wall, two different cases of jet impingement cooling process, i.e. case A and case B, are considered. Case A considers the situation where the cooling jet is directed toward any one of the ribs, while case B considers that the jet is directed toward the center line of the cavity. It is expected that the impinging jet flow and the heat transfer process along the ribbed wall for case A and case B is different. Case A is considered first.

In general, the impinging jet flow structure along a ribbed wall is significantly different from that along a flat plate. When the slot width is large and the nozzle is close to the ribbed wall, as shown in Fig. 3(a) for $b/e = 6.67$ and $z/b = 4$, upon arriving at the edge of the rib, the jet does not move into the cavity, but it turns horizontally and moves along the edge of the

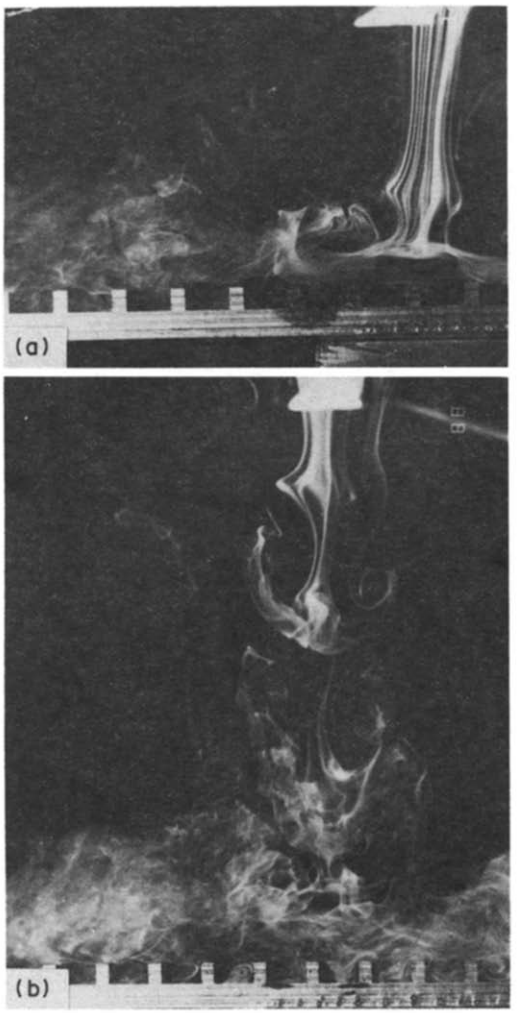

FIG. 3. Wall jet flow structure along the ribbed wall for $h/e = 6.67$, $Re = 2500$, $p/e = 4$ and (a) $z/b = 4$ and (b) $z/b = 8$.

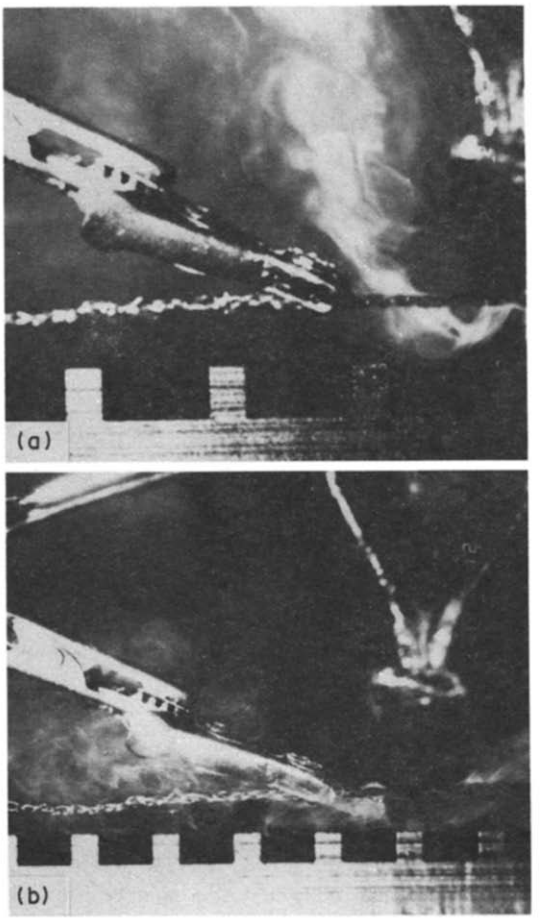

FIG. 4. Wall jet flow structure along the ribbed wall for $h/e = 1.17$, $Re = 2500$, $z/b = 4$ and (a) $p/e = 4$ and (b) $p/e = 3$.

ribs. It appears that close to the stagnation point, the pressure inside the cavity is significantly higher than outside, and formation of an air bubble enclosing the cavity occurs which prevents the air jet from penetrating into the cavity. The formation of an air bubble may occur in several cavities downstream along the wall until the wall jet becomes turbulent which can penetrate into the cavity. As the wall jet moves away from the stagnation point, the pressure inside the cavity decreases which allows penetration of a small amount of jet air from the outside. However, in the region of the laminar wall jet this could not be observed clearly in the photograph. It is expected that the amount of air penetrating and recirculating inside the cavity increases as the wall jet moves downstream. As the wall jet becomes turbulent, a relatively large amount of air penetrating and recirculating inside the cavity can be visualized clearly. Further downstream, the wall jet actually separates from the rib and reattaches, and recirculates inside the cavity. It is expected that the heat transfer at the point of reattachment can be significantly enhanced.

When the nozzle-to-plate spacing is large, as shown in Fig. 3(b) with $z/b = 8$, the jet flow before arriving at the wall becomes diffused and turbulent. The highly turbulent jet flow can penetrate the air bubble enclosing the cavity and reattach, recirculate inside, a recirculation cell inside each cavity can be observed clearly.

For a narrow slot, the jet impinging on the wall can rebound and move away from the wall, as shown in Fig. 4(a), due to the protrusion of ribs, and a vacuum can be created in the downstream region. In addition, the vacuum created can suck the air flow and make the jet move back toward and reattach to the wall again. This peculiar phenomenon does not occur for a wider slot in the case of $p/e = 3$ as shown in Fig. 4(b). For a higher p/e, i.e. $p/e \geqslant 4$, the rebound of the air jet is expected to occur for a jet from a wider slot. At this stage, the heat transfer in the downstream region where a vacuum is created is expected to reduce significantly. The rebound of the jet flow and the vacuum created downstream occurs for $z/b \leqslant 8$. As the impinging jet becomes fully turbulent and wide, i.e. at $z/b > 8$, the rebound of the jet flow does not occur. At this stage, the wall jet moves along the ribbed wall like the case of the wall jet from a wider slot.

When the jet is directed toward the center line of

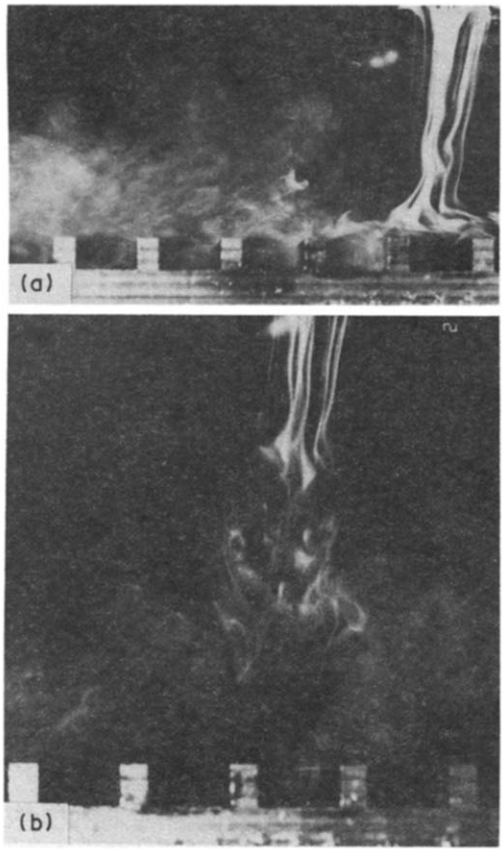

FIG. 5. Wall jet flow structure along the ribbed wall for case B with $b/e = 2$, $Re = 2500$ and (a) $z/b = 8$ and (b) $z/b = 12$.

the cavity, flow visualization of jet impingement from a narrow slot is shown in Fig. 5. When the jet is laminar before arriving at the surface, a similar kind of air bubble enclosing the cavity which prevents the penetration of the jet flow from the outside is observed. Penetration of the wall jet flow into the air bubble and recirculation cell inside the cavity is not observed until the wall jet becomes turbulent. When the nozzle-to-plate spacing z/b is large and the impinging flow before arriving at the wall becomes turbulent, the turbulent jet can penetrate into the cavity and recirculates inside, as shown in Fig. 5(b). Therefore, the impinging flow structure for case B is very similar to case A.

3.2. *Heat transfer*

3.2.1. *Effect of slot width on the flat plate heat transfer.* For the purpose of comparison, the local Nusselt number for the case of impingement cooling over a flat plate is also measured and presented in Fig. 6. The local Nusselt number has a maximum value at the stagnation point, which decreases monotonically toward downstream. When the impinging jet is laminar before arriving at the surface, a second peak in the Nusselt number occurs at a location close to $x/b = 7$, as shown in Fig. 6(a), due to the occurrence of a transition from a laminar wall jet into a turbulent one. The Nusselt number on and around the stagnation point increases, as expected, with increasing slot width. This is due to the fact that a wider slot causes an earlier initiation of vortices in the mixing region of the jet which leads to an earlier termination of the potential core and an increase in the momentum transport in the jet. The increase of the stagnation point Nusselt number with increasing slot width is also found in the work of others [1–5]. In the downstream region, however, the local Nusselt numbers for different slot widths approach approximately the same value.

Comparison of the present data with the results of others [3, 4] are also made as shown in Fig. 6. The current data agree well with the results of Schlunder in ref. [2]. However, the data of Gardon and Akfirat are significantly lower than the current data. Becko [2] mentions that the data from Gardon and Akfirat are 20% lower due to an experimental error. Therefore, a 20% increase of Gardon and Akfirat's data can make their results approach the current ones.

3.2.2. *Effect of slot width-to-rib height ratio on the local Nusselt number.* For impingement cooling over a rib-roughened wall, the protrusion of the ribs has the effect of promoting turbulence in the wall jet. In addition, the wall jet passing through the cavity can separate from the rib, reattach to the bottom, and recirculate inside the cavity. When the wall jet becomes thicker, due to an increase in slot width, the wall jet separating from the rib can reattach to the next rib and recirculate inside the cavity. Therefore, a significant enhancement in heat transfer along the ribbed wall can be expected. In addition, the protrusion of the ribs increases the local area at the location where the rib stands, which can increase the total heat transfer rate. This leads to an increase in the heat transfer coefficient that is calculated based on the base area of the rib.

However, the rib has an opposite effect in reducing the momentum in the wall jet, which leads to a reduction in heat transfer. Figure 7 shows that the local Nusselt number distribution for the ribbed wall deviates drastically from the one for a flat plate. For the purpose of comparison, the Nusselt number results over a flat plate for the slot width $b = 3.5$ mm are also plotted and presented in Fig. 7. When the slot width-to-rib height ratio is small, the wall jet layer is relatively thin as compared with the rib height, the momentum of the wall jet is significantly reduced by the ribs. This leads to a significant reduction in local Nusselt number, which is lower than the results for a flat plate. Figure 7 indicates that there are many spikes in local Nusselt number, each of which is located at the second measurement point of the thermocouple downstream in the cavity. The spikes in Nusselt number are apparently due to the wall jet that reattaches to the bottom of the cavity. At the stagnation point, the Nusselt number is significantly lower than for a flat plate. This is due to the formation of an air bubble enclosing the cavity which prevents penetration of the

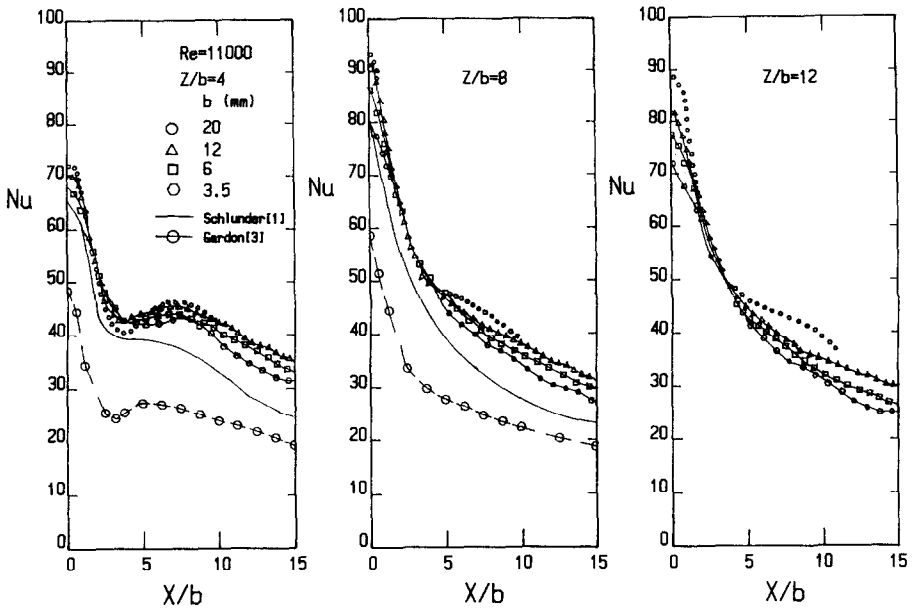

FIG. 6. Local Nusselt number for the case of flat plate and comparison with the results of others.

wall jet from the outside. This has been shown in the flow visualization experiments. Since the bubble enclosing the cavity is almost stagnant, this results in a very low value of Nusselt number. However, a significant spike in the Nusselt number at each of the second measurement points of the thermocouple downstream in the cavity suggests that some of the jet flow can penetrate the bubble and impinge on the bottom wall.

As the jet moves horizontally along the top of the ribs, the amount of jet air penetrating into the cavity increases, especially when the wall jet becomes turbulent, penetration and recirculation of the jet air inside the cavity can be clearly observed in the previous photographs. This leads to a gradual increase in the average Nusselt number which reaches a maximum at approximately $x/b = 4$. In addition, the maximum in the Nusselt number at $x/b = 4$ suggests the occurrence of a transition of the wall jet from laminar to turbulent flow and that a relatively large amount of the jet flow can penetrate the air bubble and recirculate inside the cavity. Due to the rib protrusion, however, the transition for the ribbed wall occurs at an earlier stage than for the flat wall. As the wall jet

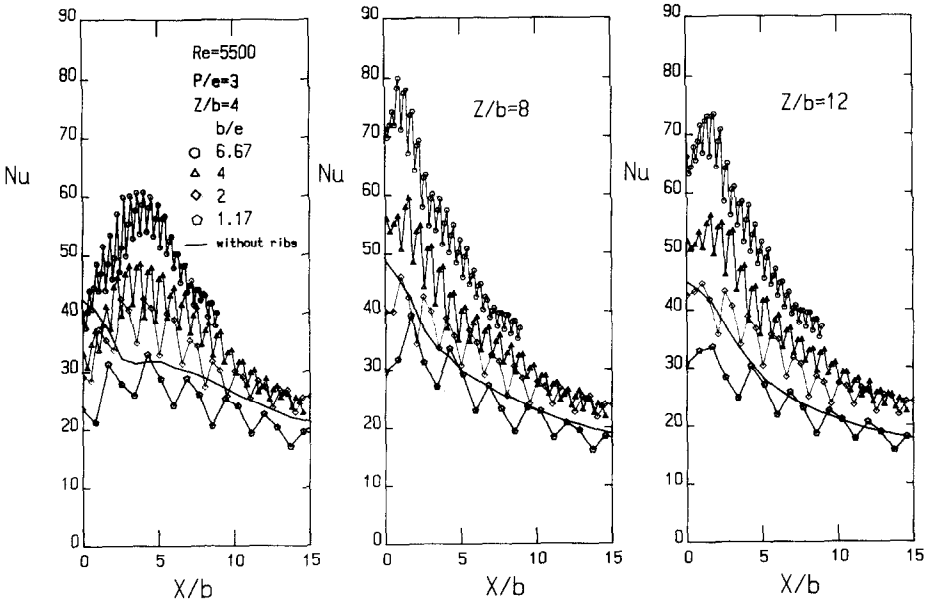

FIG. 7. Local Nusselt number distribution at different slot width-to-rib height ratios for the case of $p/e = 3$, $Re = 5500$ and (a) $z/b = 4$, (b) $z/b = 8$ and (c) $z/b = 12$.

moves further downstream along the ribbed wall, the Nusselt number decreases significantly due to the increase in the wall jet layer thickness. However, the rate of reduction in the Nusselt number along the ribbed wall is higher than along the flat plate. This is apparently due to the rib protrusion that can reduce the horizontal momentum of the wall jet. As the nozzle-to-plate spacing z/b increases and the impinging jet is turbulent before arriving at the wall, the maximum in Nusselt number moves gradually toward the stagnation point. At this stage, the maximum in Nusselt number is not due to the occurrence of a transition of the wall jet into turbulent flow. For the turbulent jet, a relatively large amount of the jet flow can readily penetrate and impinge on the bottom of the cavity and increase the heat transfer, especially in the region around the stagnation point. This has been observed in the flow visualization experiments. However, the Nusselt number at the stagnation point is still lower than in the cavity around the stagnation point, due to the effect of air bubble formation enclosing the cavity.

The increase in the slot width can gradually increase the pressure distribution in the cavity around the stagnation point. This leads to the result that penetration of the impinging jet into the air bubble enclosing the cavity becomes relatively difficult and the heat transfer inside the cavity around the stagnation point is lower than at the stagnation point. This is also true when the nozzle is far away from the plate and the impinging jet becomes turbulent before arriving at the plate.

For a wider slot, the wall jet is thicker, and the protrusion of the ribs becomes relatively small as compared with the wall jet thickness. The local Nusselt number at the location where the rib stands starts to increase while the one at the second measurement point downstream in the cavity decreases. For the case when $b/e \geqslant 4$, the spike in Nusselt number occurs frequently at the location where the rib stands, as shown in Fig. 7. This is due to the fact that the thicker wall jet can impinge on and reattach to the next rib as it separates from the previous rib.

As the slot width increases, the average Nusselt number increases rapidly with an increasing slot width-to-rib height ratio, especially when the jet impinging on the wall is turbulent or when a transition of the wall jet from laminar to turbulent flow occurs (i.e. at $x/b = 4$). For the case when $b/e \geqslant 2$, the Nusselt number results along the ribbed wall are significantly higher than along the flat plate. However, when the impinging jet is laminar, which can create an air bubble enclosing the cavity near the stagnation point, the Nusselt number there is lower than for the flat plate. When the Reynolds number increases, the Nusselt number distribution along the ribbed wall is very similar, as shown in Fig. 8, except that the local spike in the Nusselt number is higher. This fact indicates that the impingement and the reattachment of the wall jet on the rib or on the bottom of the cavity can enhance the heat transfer more effectively at a higher Reynolds number than at a lower one.

For the case when the cavity width increases, the spike in the Nusselt number occurs, in general, at the location where the rib stands, as shown in Fig. 9 for $p/e = 4$, even when the value of b/e is relatively small. The spikes in the Nusselt number for $p/e = 4$ are significantly higher than for $p/e = 3$. This is due to the fact that the amount and the velocity of the wall jet penetrating into the cavity are higher for $p/e = 4$ than for $p/e = 3$. As the slot width increases, the local spikes of the Nusselt number at the ribs increase significantly. However, the rate of increase of the average Nusselt number distribution with the slot width for $p/e = 4$ is not as rapid as that for $p/e = 3$. This fact suggests that as p/e increases, the effect of the slot width on the average heat transfer distribution approaches the results of a flat plate. However, the maximum in the average Nusselt number for $z/b = 4$ occurs approximately at $x/b = 3$. It appears that the transition of the wall jet from laminar to turbulent flow for a wider cavity can occur at an earlier stage than for a narrow one.

For $z/b \geqslant 8$, the maximum in average Nusselt number moves gradually toward the stagnation point. When the cavity becomes wide, the impinging flow can more readily penetrate the air bubble enclosing the cavity and impinge on the wall. This causes a significantly higher heat transfer in the stagnation point than in the region around the stagnation point.

However, a peculiar phenomenon occurs for the case when $b/e = 1.17$. The maximum in averaging the Nusselt number distribution does not occur at the condition when the nozzle-to-plate spacing is 8 but does when $z/b = 12$. This is due to the fact that when the nozzle-to-plate spacing is small, i.e. $z/b \leqslant 8$, the jet impinging on the wall rebounds backwards and a vacuum can be created in the downstream region, as shown in the previous flow visualization. The occurrence of a vacuum downstream of the rebounding jet for $z/b \leqslant 8$ leads to the result that the Nusselt number in that region is relatively low. When $z/b = 12$, the rebound of the air jet does not occur, and the wall jet moves horizontally along the ribbed wall. The Nusselt number at the current stage increases significantly so that the average Nusselt number is even higher than for the case along a flat plate.

When the impinging jet is directed toward the center line of the cavity, the Nusselt number distribution is very similar to the case when the impinging jet is directed toward the rib, as shown in Fig. 10, except in the region around the stagnation point where the Nusselt number is significantly low. This is due to the formation of an air bubble enclosing the cavity around the stagnation point that prevents the air jet from impinging on the wall. As the slot width increases, which leads to an increase of the pressure distribution around the stagnation point, this makes the penetration of the jet into the cavity more difficult, even when the jet becomes turbulent before arriving at the

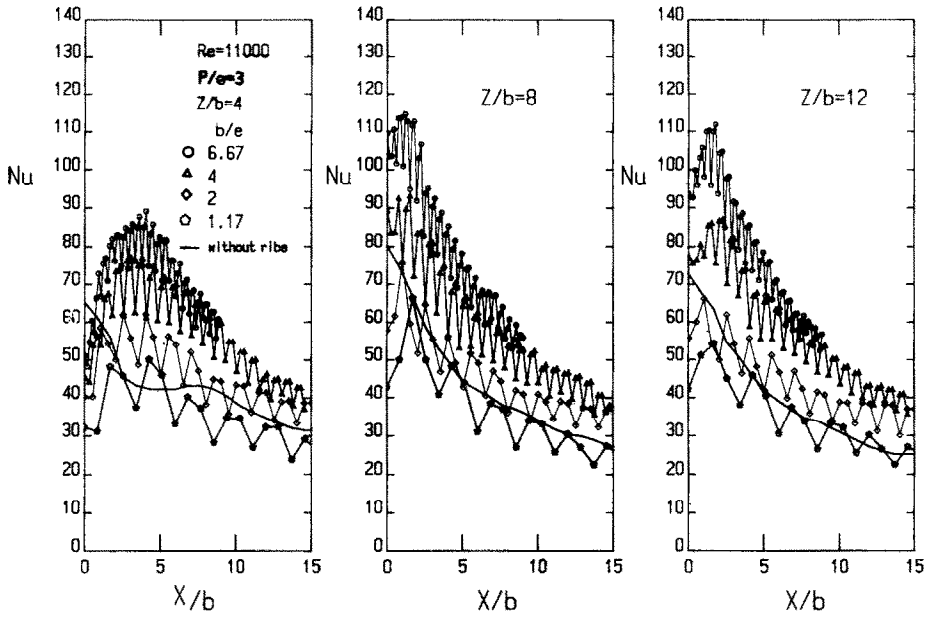

FIG. 8. Local Nusselt number distribution at different slot width-to-rib height ratios for the case of $p/e = 3$, $Re = 11\,000$ and (a) $z/b = 4$, (b) $z/b = 8$ and (c) $z/b = 12$.

wall. Therefore, the Nusselt number at the stagnation point is lower than in the region around the stagnation point. For the case of $b/e = 1.17$, due to the occurrence of an air bubble enclosing the cavity around the stagnation point, the jet impinging on the wall does not rebound and create a vacuum, but it moves horizontally along the ribbed wall. Therefore, the Nusselt number distribution in the downstream region for $z/b \leqslant 8$ is higher than in the case when the jet is directed toward the rib.

3.2.3. *Stagnation point Nusselt number.* The stagnation point Nusselt number for the case of the ribbed wall is compared with the case of the flat plate as shown in Fig. 11. The stagnation point Nusselt number for both the ribbed wall and the flat plate increases with increasing slot width. However, due to the formation of the air bubble enclosing the cavity around the stagnation point, which can prevent the impinging jet from penetrating into the bubble, the stagnation point Nusselt number for the ribbed wall is much lower than for the flat plate. This is true for the jet issued from a narrow slot, or a wider slot when z/b is less than 8. When the slot width becomes wider and the impinging jet becomes turbulent before arriving at the wall, the jet can readily penetrate the air bubble and impinge on the wall. This can significantly increase the stagnation point Nusselt number which is higher than in the case of a flat plate. The maximum Nusselt number at the stagnation point for the ribbed wall occurs at the nozzle-to-plate spacing $z/b = 10$, while for the flat plate it occurs at $z/b = 8$. This is apparently due to the effect of rib protrusion and the formation of an air bubble enclosing the cavity. At high Reynolds numbers, a similar distribution of stagnation point Nusselt number is found except that for $b/e \leqslant 2$, the Nusselt number is relatively low due to formation of an air bubble [17].

The stagnation point Nusselt numbers for $p/e = 3$ and $p/e = 4$ are compared in Fig. 12, both of which increase with increasing b/e. However, the stagnation point Nusselt number for $p/e = 3$ is, in general, lower than for $p/e = 4$. This is due to the fact that the air bubble enclosing the cavity around the stagnation point for $p/e = 4$ is relatively large as compared with the case for $p/e = 3$ when the impinging jet can more readily penetrate the air bubble and impinge on the wall. This leads to a higher Nusselt number at and around the stagnation point for $p/e = 4$. The maximum Nusselt number at the stagnation point for both $p/e = 3$ and $p/e = 4$ occurs at $z/b = 10$. For the case of $b/e = 6.67$, the stagnation point Nusselt number for both $p/e = 3$ and $p/e = 4$ approaches the same value. Similar results have been obtained for a higher Reynolds number, except that the maximum in the stagnation point Nusselt number for $b/e = 6.67$ occurs at $z/b = 8$, which approaches the results of the flat plate [17].

The stagnation point Nusselt numbers for the case when the impinging jet is directed toward the rib and the case when it is directed toward the center line of the cavity are compared in Fig. 13. In general, the stagnation point Nusselt number for case A is higher than for case B. This is due to the fact that the impinging jet for case A can more readily penetrate the air bubble enclosing the cavity and impinge on the wall. In addition, the protrusion of the ribs increases the local surface area at the location where the rib stands, which can increase the total heat transfer rate and the heat transfer coefficient that is calculated based on the base area of the rib. For case B, however,

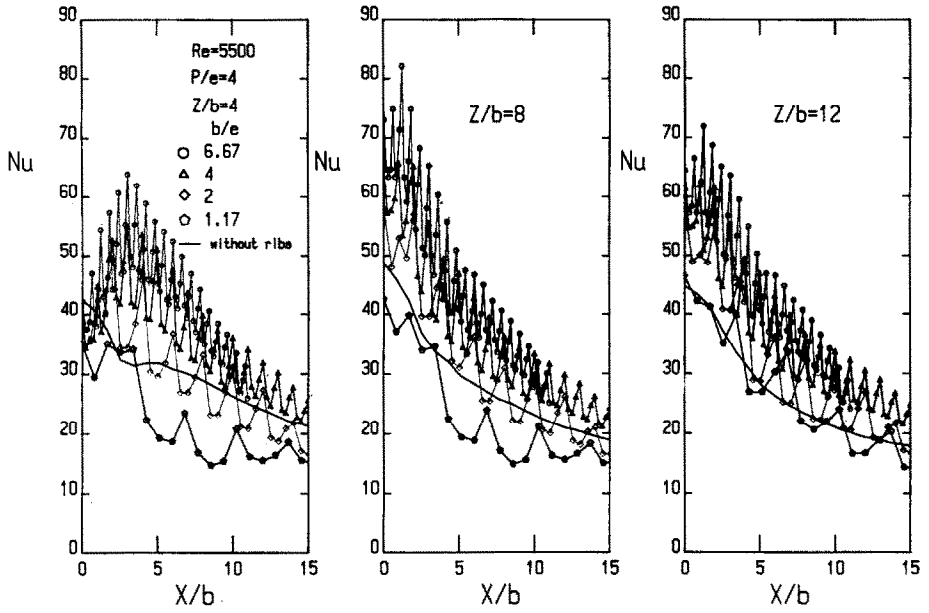

FIG. 9. Local Nusselt number distribution at different slot width-to-rib height ratios for the case of $p/e = 4$, $Re = 5500$ and (a) $z/b = 4$, (b) $z/b = 8$ and (c) $z/b = 12$.

the maximum Nusselt number at the stagnation point for higher values of b/e occurs approximately at $z/b = 8$, which approaches the results of the flat plate; while that for lower values of b/e occurs at $z/b = 10$, which approaches the results of the ribbed wall. This is also true at higher Reynolds numbers [17].

3.2.4. *Correlation of stagnation point Nusselt number.* The stagnation point Nusselt number increases monotonically with an increasing slot width-to-rib height ratio at both low and high Reynolds numbers. Correlations of Nu_o in terms of the Reynolds number, the slot width-to-rib height ratio, the nozzle-to-plate spacing and the rib pitch-to-height ratio can be made. However, better correlations can be obtained as follows if the correlations for $z/b \leqslant 10$ and $z/b \geqslant 10$ are made separately:

For case A with $2 \leqslant z/b \leqslant 10$, the least square fit of data is

$$Nu_o = 0.143(b/e)^{0.32}(p/e)^{0.57}(Re)^{0.5}(z/b)^{0.34} \quad (2)$$

where the standard deviation of the data is 0.05.

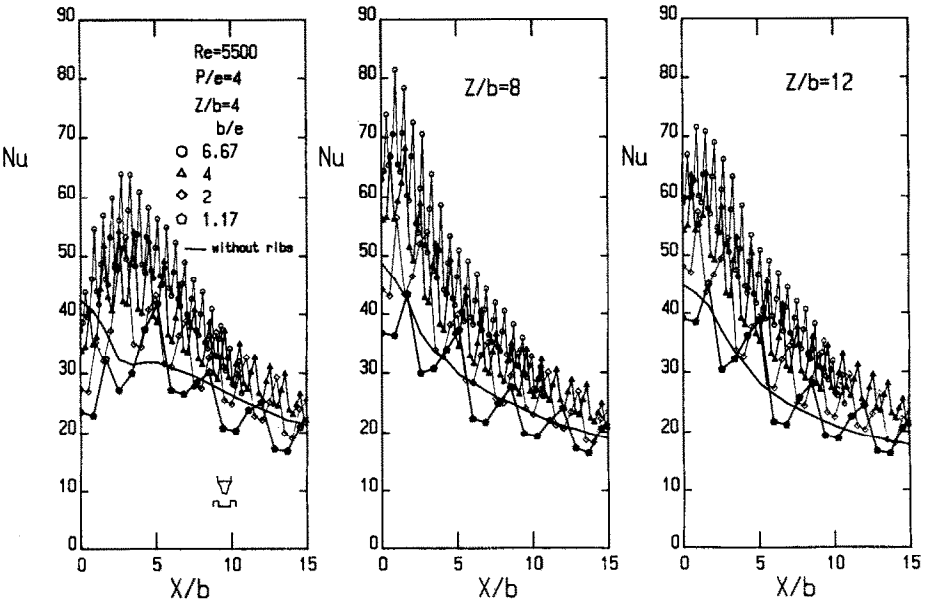

FIG. 10. Local Nusselt number distribution at different slot width-to-rib height ratios for case B with $p/e = 4$, $Re = 5500$ and (a) $z/b = 4$, (b) $z/b = 8$ and (c) $z/b = 12$.

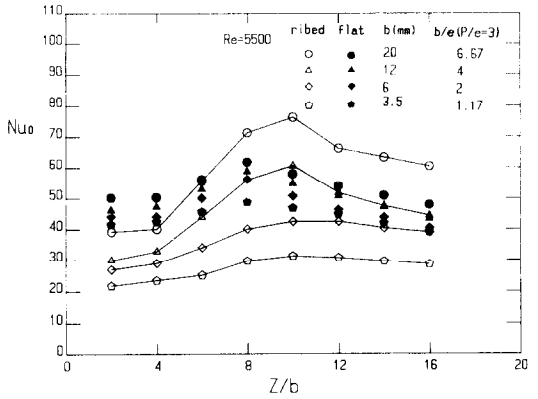

FIG. 11. Comparison of stagnation point Nusselt number between the case of flat plate and the case of ribbed wall for $Re = 5500$.

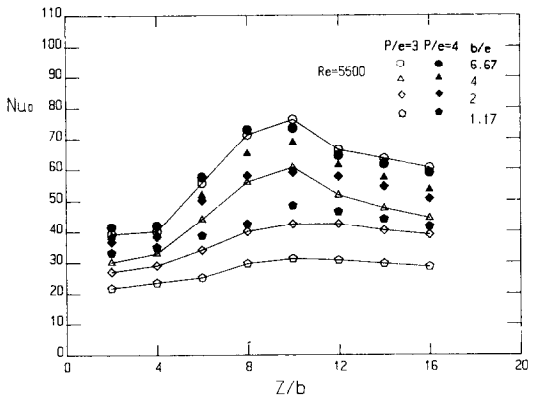

FIG. 12. Comparison of stagnation point Nusselt number between the case of $p/e = 3$ and the case of $p/e = 4$ for $Re = 5500$.

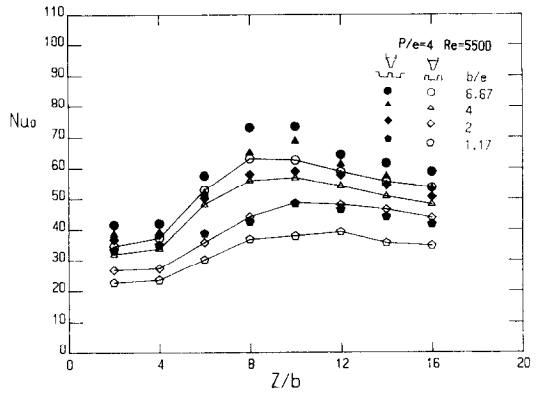

FIG. 13. Comparison of stagnation point Nusselt number between case A and case B for $Re = 5500$.

For case A with $10 \leqslant z/b \leqslant 16$,

$$Nu_o = 0.639(b/e)^{0.33}(p/e)^{0.53}(Re)^{0.51}(z/b)^{-0.32} \quad (3)$$

where the standard deviation of the data is 0.04.

For case B with $2 \leqslant z/b \leqslant 8$,

$$Nu_o = 0.154(b/e)^{0.33}(p/e)^{0.22}(Re)^{0.50}(z/b)^{0.37} \quad (4)$$

where the standard deviation of the data is 0.04.

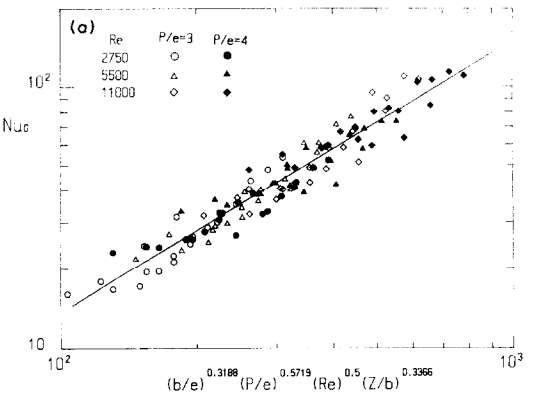

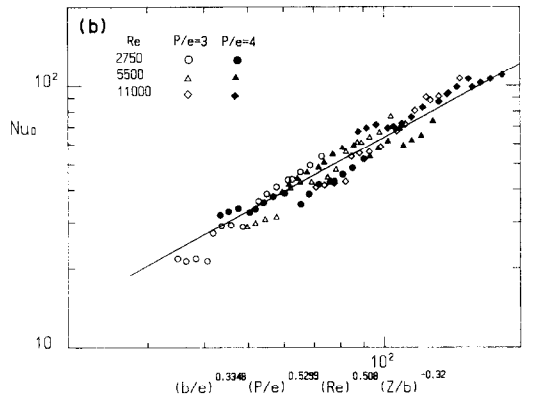

FIG. 14. Correlation of the stagnation point Nusselt number for case A with $2500 \leqslant Re \leqslant 11000$, $1.17 \leqslant b/e \leqslant 6.67$, $3 \leqslant p/e \leqslant 4$, and (a) $2 \leqslant z/b \leqslant 10$, (b) $10 \leqslant z/b \leqslant 16$.

For case B with $8 \leqslant z/b \leqslant 16$,

$$Nu_o = 0.335(b/e)^{0.31}(p/e)^{0.2}(Re)^{0.51}(z/b)^{-0.11} \quad (5)$$

where the standard deviation of the data is 0.02.

The above correlations are valid for $2500 \leqslant Re \leqslant 11000$, $1.17 \leqslant b/e \leqslant 6.67$ and $3 \leqslant p/e \leqslant 4$. In addition, the above correlations indicate that the stagnation point Nusselt number for case A is more sensitive to the change of p/e than for case B, since the power of p/e in equation (2) for case A is significantly larger than in equation (4) for case B. The fact that Nu_o is proportional to the Reynolds number to the one half power for $z/b \leqslant 10$ agrees with the analysis from Hrycak [13] and the experimental correlation of others [3, 4] for the case of flat plate. The typical least square fit of data is presented in Figs. 14(a) and (b).

4. CONCLUSIONS

An experimental study of the impinging jet flow structure and heat transfer along the rib-roughened walls is made, the results are significantly different from the ones along a flat plate. Due to the protrusion of the ribs, the formation of an air bubble enclosing the cavity is visualized which can prevent the jet flow from impinging on the wall and reduce the heat trans-

fer. However, some of the jet flow along the top of the rib in the downstream region, especially when it becomes turbulent, can penetrate the air bubble and impinge, and recirculate inside the cavity, which can significantly increase the heat transfer. An increase of the slot width-to-rib height ratio leads to the results that the wall jet can separate from the rib, reattach to the next one and recirculate inside the cavity. The reattachment and recirculation of flow can significantly enhance the heat transfer, especially at the location where the rib stands.

In addition, the effect of the Reynolds number, the gap width-to-rib height ratio and the location of the impinging jet on the flow and heat transfer along the ribbed wall is also studied. It is found that the Nusselt number at the stagnation point is relatively low and is significantly affected by these parameters. The maximum in the stagnation point Nusselt number occurs mostly at approximately $z/b = 10$, which is different from the results of a flat plate. Correlations of the stagnation point Nusselt number for the jet directed at both the rib and the center line of the cavity are obtained.

Acknowledgement—This research was sponsored by the National Science Council of Taiwan under contract No. NSC 81-0401-E-006-624.

REFERENCES

1. H. Martin, Heat and mass transfer between impinging gas jets and solid surfaces. In *Advances in Heat Transfer* (Edited by J. Hartnett and T. Irvine, Jr.), Vol. 13, pp. 1–60 (1977).
2. Y. Becko, Impingement cooling—a review, Von Karman Institute for Fluid Dynamics, Lecture Series 83 (1976).
3. R. Gardon and J. C. Akeirat, Heat transfer characteristics of impinging two-dimensional air jet, *ASME J. Heat Transfer* **88,** 101–108 (1966).
4. M. Korger and F. Krizek, Mass-transfer coefficient in impingement flow from slotted nozzles, *Int. J. Heat Mass Transfer* **9,** 337–344 (1981).
5. R. Gardon and J. Cobonpue, Heat transfer between a flat plate and jets of air impinging on it. In *Int. Dev. Heat Transfer, Proc. 2nd Int. Heat Transfer Conf.*, ASME, New York, pp. 454–460 (1963).
6. R. J. Goldstein and M. E. Franchett, Heat transfer from a flat surface to an oblique impinging jet, *ASME J. Heat Transfer* **110,** 84–90 (1988).
7. R. J. Goldatein and J. F. Timmers, Visualization of heat transfer from arrays of impinging jets, *Int. J. Heat Mass Transfer* **25,** 1857–1868 (1982).
8. J. W. Baughn and S. Shimizu, Heat transfer measurements from a surface with uniform heat flux and an impinging jet, *ASME J. Heat Transfer* **111,** 1097–1100 (1989).
9. C. D. Donaldson and R. S. Snedeker, A study of free jet impingement, Part 1: mean properties of free impinging jets, *J. Fluid Mech.* **45,** 281–319 (1971).
10. C. D. Donaldson and R. S. Snedeker, A study of free jet impingement, Part 2: free jet turbulence structure and impingement heat transfer, *J. Fluid Mech.* **45,** 477–512 (1971).
11. P. Hrycak, Heat transfer from round impinging jets to a flat plate, *Int. J. Heat Mass Transfer* **26,** 1857–1865 (1983).
12. D. E. Metzger, T. Yamashita and C. W. Jenkins, Impingement cooling of concave surfaces with lines of circular air jets, *ASME J. Engng Power* **91,** 149–158 (1969).
13. P. Hrycak, Heat transfer from a row of impinging jets to concave cylindrical surfaces, *Int. J. Heat Mass Transfer* **24,** 407–419 (1980).
14. W. Tabakoff and W. Flevenger, Gas turbine blade heat transfer augmentation by impinging air jets having various configurations, *ASME J. Engng Power* **94,** 51–60 (1972).
15. C. Gau and C. M. Chung, Surface curvature effect on slot-air-jet impingement cooling flow and heat transfer process, *ASME J. Heat Transfer* **113,** 858–864 (1991).
16. H. A. Becker and T. A. Massaro, Vortex evolution in a round jet, *J. Fluid Mech.* **31,** 435–448 (1968).
17. C. C. Lee, Impingement cooling heat transfer along rib-roughened walls, M.S. thesis, National Cheng Kung University, Taiwan, Republic of China (1991).

STRUCTURE D'UN ECOULEMENT IMPACTANT ET TRANSFERT THERMIQUE LE LONG DES PAROIS NERVUREES

Résumé—On étudie expérimentalement la structure de l'impaction d'un jet d'air sortant d'une fente et le transfert thermique le long de parois nervurées. L'écoulement est visualisé avec de la fumée formée en vaporisant l'huile déposée sur un film chauffé. L'effet des protusions (hauteurs) des nervures sur l'écoulement impactant et le transfert thermique est étudié en considérant plusieurs tailles d'injecteur. On choisit deux parois nervurées avec différents pas de nervures et avec un rapport pas/hauteur de 3 et 4. Le nombre de Reynolds varie de 2500 à 11 000, le rapport largeur de la fente/hauteur de la nervure allant de 1,17 à 6,67 et la distance fente-plaque allant de 2 à 16. A cause de la hauteur de la nervure, il se forme une bulle d'air entourant la cavité, ce qui empêche le jet de frapper la paroi et ce qui réduit le transfert thermique. Toutefois dans la région en aval, spécialement quand l'écoulement devient turbulent, celui-ci recircule dans la cavité, ce qui accroît fortement le transfert thermique. En général la structure de l'écoulement et le transfert thermique observés sont significativement différents du cas d'une plaque plane. Une comparaison et des formules pour le Nusselt au point d'arrêt sont présentées et discutées.

STRUKTUR UND WÄRMEÜBERGANG IN EINER AUF EINE BERIPPTE WAND AUFTREFFENDEN, KÜHLENDEN STRÖMUNG

Zusammenfassung—Struktur und Wärmeübergang in einem schlitzförmigen Luftstrahl, der auf eine berippte Wand auftrifft, wird experimentell untersucht. Die Strömung wird mit Rauch sichtbar gemacht, der durch Verdampfen von Öl an der Oberfläche eines beheizten Drahtes erzeugt wird. Der Einfluß unterschiedlicher Rippenhöhen auf Strömung und Wärmeübergang entlang der Wand wird untersucht. Hierfür werden unterschiedliche Düsenabmessungen verwendet. Zwei Wandgeometrien mit unterschiedlichen Teilungsverhältnissen der Rippen (Verhältnis von Rippenabstand zu Rippenhöhe 3 und 4) wurden ausgewählt. Die Reynolds-Zahl wird zwischen 2500 und 11 000 variiert, das Verhältnis von Schlitzbreite zu Rippenhöhe zwischen 1,17 und 6,67 und das Verhältnis des Düsenabstandes zum Rippenabstand zwischen 2 und 16. Infolge der Rippen kann eine Stagnationszone in den Vertiefungen zwischen den Rippen entstehen, die ein Auftreffen des Strahls auf die Wand verhindert und dadurch den Wärmeübergang beeinträchtigt. Andererseits kann ein Teil des Strahls in die Stagnationszone eindringen, auf die Wand auftreffen und eine Zirkulationsströmung in der Stagnationszone hervorrufen, was den Wärmeübergang verbessert. Dies gilt vor allem, wenn die Strömung turbulent wird. Im allgemeinen unterscheiden sich die Strömungsstruktur und der Wärmeübergang deutlich von denjenigen für eine ebene Platte. Die Nusselt-Zahl am Stagnationspunkt wird für unterschiedliche Bedingungen verglichen und korreliert.

СТРУКТУРА НАБЕГАЮЩЕГО ОХЛАЖДАЮЩЕГО ПОТОКА И ТЕПЛОПЕРЕНОС У ОРЕБРЕННЫХ СТЕНОК

Аннотация—Экспериментально исследуются структура набегающей охлаждающей плоской струи воздуха и теплоперенос у оребренных стенок. Проводится дымовая визуализация структуры течения вдоль оребренной стенки, осуществляемая за счет испарения масла, покрывающего проволоку. С использованием сопел различных размеров исследуется влияние различной высоты ребер на набегающий поток и теплоперенос у стенки. Выбраны два вида оребрения стенки с различным расстоянием между ребрами и отношением этого расстояния к высоте, составляющим соответственно 3 и 4. В процессе экспериментов число Рейнольдса изменяется от 2500 до 11 000, отношение ширины к высоте ребра—от 1,17 до 6,67, а расстояния между соплом и пластиной—от 2 до 16. Благодаря наличию ребер происходит образование воздушного пузырька, что может препятствовать набеганию струи на стенку и снижать теплоперенос. Однако некоторая часть струйного течения на участке, расположенном вниз по потоку, особенно при его турбулизации, может проникать в воздушный пузырек и попадать на стенку, а также рециркулировать в полости, что приводит к существенной интенсификации теплопереноса. Таким образом, полученные данные по структуре течения и теплопереносу значительно отличаются от результатов для плоской пластины. Приводятся и обсуждаются результаты сравнения и обобщающие соотношения для числа Нуссельта в точке торможения.